nature geoscience
SUPPLEMENTARY INFORMATION
DOI: 10.1038/NGEO1557

Deep Arctic Ocean warming during the last Glacial Cycle

T. M. Cronin, G. S. Dwyer, J. Farmer, H. A. Bauch, R. F. Spielhagen, M. Jakobsson, J. Nilsson, W. M. Briggs, Jr., A. Stepanova

Mg/Ca and Sr/Ca ratios in ostracods

Mg/Ca ratios in adult valves of the benthic ostracod *Krithe glacialis* and *K. minima* are preferred for palaeothermometry and BWT reconstruction due to ostracod growth by moulting in which the shell is secreted from ambient water (Turpen and Angell, 1971), common preservation of adult valves in the Arctic (Cronin et al., 1996), field and laboratory temperature dependence of Mg/Ca ratios in marine ostracods (Dwyer et al., 1995) and the absence of a carbonate ion effect that might affect benthic foraminiferal Mg/Ca ratios at colder temperatures (Farmer et al., 2012). The Mg/Ca-temperature relationship for *K. glacialis* based on Arctic-Nordic Sea coretop material from 50 sites (50 to 3500m water depth, temperatures from -1.6º to 1ºC) is expressed in the equation

$$BWT\ (ºC) = (0.438 \times Mg/Ca_{Kg}) - 5.14 \qquad (r^2 = 0.5) \qquad (1)$$

This calibration has a 1σ prediction error of ±1.0°C (Fig. S1) (Farmer et al., 2012) and a temperature sensitivity is ~ 2.3mmol mol^{-1} $ºC^{-1}$. This sensitivity is nearly double that of *Krithe* species from the North Atlantic (temperature range of 2º to 14ºC) (Dywer et al., 1995) but similar to that from Coral Sea *Krithe* Mg/Ca (temperatures 2º to 6ºC) (Corrège and De Deckker, 1997).

Figure S2 presents a depth profile Arctic coretop Mg/Ca_{Kg} data using only samples with > 3 Mg/Ca measurements, showing standard deviation for each sample and colour-coding the Nordic, Eurasian and Amerasian Basin samples. The within-sample scatter in Mg/Ca ratios at some intermediate and deep-sea sites in the Amerasian Basin can be due to several factors. Sedimentation rates in the deep Arctic average ~1 cm kyr^{-1} (Backman et al., 2004), such that the uppermost 1 or 2 cm of coretop sediment represents a time-averaging of a few thousand years. It is doubtful that temporal changes in deep

Arctic Ocean temperatures could cause this variability, although it cannot be totally ruled out. Other environmental factors affecting *Krithe* growth and population ecology, such as food supply, may have caused the within-sample variability.

In addition to calculating regression equations for Mg/Ca_{Kg} across a range of water temperatures, another way to examine patterns in Mg/Ca_{Kg} and Sr/Ca_{Kg} ratios is to plot coretop Mg/Ca values in a cross-section of Arctic-Nordic Sea water masses (Figure S3). This illustrates a first order relationship showing low Mg/Ca_{Kg} values (~7-9 mmol/mol) in the shallow Polar Mixed Layer (PML) and higher values (9->12 mmol/mol) in the Atlantic Layer (AL), Arctic Intermediate Water (AIW), and upper Eurasian and Amerasian Deep Water (EBDW, ABDW). Only a few stations are located in the core of the AL and additional work is needed in this water mass especially where the AL enters the Arctic near the Fram Strait. Nonetheless, relatively high values in AIW at 500-1500 m in the Eurasian Basin and 1000-2500 m in the Amerasian Basin are consistent with modern bottom temperature patterns. Mg/Ca values are lower in EBDW below about 1500m and ABDW below ~2500-3000 m in the Amerasian Basin, except in a few abyssal plain samples.

Sr/Ca ratios in ostracods are used for paleoenvironmental reconstruction in shallow marine, brackish or freshwater systems (Chivas et al., 1986; De Deckker et al., 1999; Holmes and Chivas, 2002). Sr/Ca_{Kg} from Arctic coretops shows the opposite pattern as that of Mg/Ca_{Kg} such that the highest Sr/Ca_{Kg} values are seen in the PML and the lowest in EBDW and ABDW in Arctic abyssal plains (Fig. S3C). An inverse relationship between Mg/Ca_{Kg} and Sr/Ca_{Kg} is also observed in downcore specimens (r^2 = 0.5). Based on laboratory culturing experiments (Dwyer et al., 2002) and field (Chivas et al., 1983), low (high) Mg/Ca (Sr/Ca) ratios are negatively (positively) correlated with shell weight, a pattern attributed to temperature effects during moulting in which less adult shells growing in warmer water are less calcified (Dwyer et al., 2002).

A comparison of Marine Isotope Stage 3 (MIS3) mean Mg/Ca values for each central Arctic core with those for MIS1 (Holocene) reveal higher MIS3 values in *K. glacialis* (left side Fig S4) at intermediate water depths. Although fewer core sites contained *K. minima* and a direct Mg/Ca-temperature calibration is not available for this

species, Mg/Ca_{Km} values are also higher during MIS3. These patterns suggest warmer temperatures in AIW during MIS 3 than during MIS1.

Figure S5 shows downcore plots of Mg/Ca_{Kg} and Sr/Ca_{Kg} (blue lines) from six sites on the Lomonosov (HLY0503-18tc, PS2185-4), Gakkel (PS2163-1), and Mendeleyev (P1-94AR-BC8, P1-94AR-BC19B) Ridges and the Iceland Plateau (PS1243-1/2). The x-axis is inverted for the Sr/Ca_{Kg} curves. Three cores also show patterns for Mg/Ca_{Km} and Sr/Ca_{Km} with red lines. Radiocarbon ages indicate these records cover the last 40-50 ka, the LGM interval is indicated. Despite different sedimentation rates at each site, a pattern of relatively low (high) Mg/Ca (Sr/Ca) values change to maximum values followed by a post-LGM decrease (increase) in Mg/Ca (Sr/Ca). The inverse relationship between Mg/Ca and Sr/Ca values is similar to that seen in the coretop analyses. It can also be seen that in the 3 cores where both species co-occur, Mg/Ca_{Kg} values are lower than Mg/Ca_{Km} values from the same horizons. In core P1-94AR-BC8 where both species were common, Mg/Ca_{Kg} ratios (n=65) were 77% those from Mg/Ca_{Km} (n=18) and this relationship was used to correct Mg/Ca_{Km} in the composite curve in Figure 3 of the paper.

Arctic core chronology

Age models for central Arctic cores are based on 199 radiocarbon dates mostly on planktonic foraminifera species *Neogloboquadrina pachyderma* discussed in detail in Poirier et al. (2012). Dates were calibrated using the CALIB 6.0 program with the MARINE09 402-year reservoir correction curve (Stuiver and Reimer, 2010). In addition to the global marine correction of 402 years, we followed Hanslik et al. (2010) and used an additional ΔR regional correction of 300 years for radiocarbon ages < 10 ka, and a ΔR of 1000 years for ages > 10 ka. Sixty-four dates are from MIS3 (~50-29 ka), 109 dates from the deglacial through the Holocene MIS1 (~15 ka-present), and 15 dates from glacial MIS2. The lack of MIS 2 radiocarbon dates in the Arctic Ocean suggests little or no sedimentation in the central Arctic Ocean during the Last Glacial Maximum (LGM: ~22 ka ± 2) due to thick ice cover (Nørgaard-Pederson et al., 2003; Polyak et al., 2004; Polyak et al., 2009; Hanslik et al., 2010). The average two standard-deviation error on calibrated ages older than 40 ka was ±1,648 years; for ages 39 ka to 20 ka, ±1,003 years;

and ages 20 ka to recent ± 199 years. Eleven dates with infinite ages (including some published ages of >40 ka) were not used in age models.

A conceptual model of the Arctic Ocean cold halocline

The present-day stratification of the Arctic Ocean has three distinct layers (Aagaard et al. 1981, Rudels, 1995): A near-freezing point upper layer composed of low salinity surface water above the cold halocline; the intermediate Atlantic layer of warmer and more saline water; and the cold deep-water layer (Fig. S6). The physical features that control the depth of the near-freezing point upper layer can be qualitatively examined with an analytical two-layer model (Stigebrandt, 1981; Nilsson and Walin, 2010; Jakobsson et al., 2010), which describes the interaction between the upper layer and the underlying Atlantic water. In the model, the export of upper-layer water from the Arctic is denoted M. Since M is much larger than the freshwater input F to the upper layer, the conservation of salinity is to a good approximation given by

$$\Delta S\, M = S_0\, F \qquad (1)$$

where ΔS is the salinity difference between the Atlantic water and the upper layer and $S_0 = 35$ is a constant reference salinity. The volume of the upper halocline layer, given by its surface area (A) multiplied by its depth (H), is in a steady state determined by a balance between the volume export from the Arctic and turbulent mixing that acts to deepen the upper layer by incorporating underlying Atlantic water. The export of water, occurring chiefly through the Fram Strait, is geostrophically controlled (Stigebrandt, 1981), whereas the upwelling of the Atlantic water into the upper layer is proportional to the energy input from the wind to turbulent mixing (denoted ε per unit area) and inversely proportional to the halocline depth (H) and the density difference between the upper layer and the Atlantic layer (Δρ) (Kato and Phillips, 1969). Solving for the steady-state upper-layer depth and the volume export, one obtains (Nilsson and Walin, 2010)

$$H = (A\varepsilon\, 2\rho_0 f / g^2\, \Delta\rho^2)^{1/3} \qquad (2)$$

$$M = (A^2\varepsilon^2 / g^2 \rho_0 f\, \Delta\rho)^{1/3} \qquad (3)$$

where f is the Coriolis parameter, g the acceleration of gravity, and $\rho_0 = 1000$ kg m^{-3} a constant reference density. The density difference is given by

$$\Delta\rho = \beta\,\rho_0\,\Delta S - \Delta\rho_T \quad (4)$$

where β is the haline expansion coefficient and $\Delta\rho_T$ is the thermal density difference between water in the upper layer, which is assumed to be close to the freezing point, and the Atlantic layer.

A key result is that the upper cold halocline layer becomes deeper when the density difference between the upper layer and the Atlantic layer is decreased. To illustrate how the depth of the cold halocline layer in the model depends on the freshwater input and the temperature of the Atlantic water, we take $A \approx 9{\cdot}10^{12}$ m^2 and $\varepsilon \approx 10^{-3}$ W m^{-2}, values which are representative for the present-day Arctic Ocean (Jakobsson, 2002; Jakobsson et al., 2007). Figure S7 shows the dependence of the cold halocline depth and the layer salinity difference as a function of the freshwater input for three different temperatures of the Atlantic layer (1, 3, and 5°C). For Arctic freshwater inputs in the range 0.2 to 0.25 Sv (Dickson et al., 2007), the two-layer model yields a halocline depth of about 200 m and a salinity difference of about 2.5, numbers that are broadly consistent with observations (Rudels, 1995). Interestingly, the halocline depth increases when the freshwater supply decreases. Thus the two-layer model predicts that in a cold glacial climate, for which the hydrological cycle and the freshwater input is expected to be weaker (Held and Soden, 2006), the near-freezing point upper layer should be deeper. Furthermore, the deepening of the upper layer should be more pronounced if the Atlantic layer is warmer.

Another interesting feature of the model is that the cold halocline is expected to break down if the layer density difference decreases below a threshold value; stability requires that $\Delta\rho > 0.5\Delta\rho_T$ (Nilsson and Walin, 2010). Thus, the model predicts that the cold halocline, which shields the sea ice from the warm Atlantic water, becomes unstable well before convective overturning occurs, which happens first when $\Delta\rho < 0$. We underline that the model predictions are qualitative and that the stability threshold and the existence of two stable states depend on the features of the turbulent mixing. However, the key qualitative result that a reduced freshwater input or an increased Atlantic layer temperature yields a deeper halocline is insensitive to the detailed nature of the turbulent mixing (Nilsson and Walin, 2001).

Supplementary Figures

Figure S1. Mg/Ca-bottom water temperature (BWT) regression calibration: BWT (ºC) = (0.438 x Mg/Ca) – 5.14 (Farmer et al, 2012).

Figure S2. Mean Mg/Ca ratios for Late Holocene *Krithe glacialis* from sites in the Eurasian Basin (red), Amerasian Basin (blue) and Nordic Sea (green) plotted against water depth [samples with ≥3 specimens]. Horizontal lines are standard deviations.

Figure S3. A. Arctic-Nordic Sea temperature section from Ocean Data View. B. Cross section across Arctic and Nordic Seas *Krithe glacialis* Mg/Ca and C. *Krithe glacialis* Sr/Ca ratios from coretops from 126 sites. Metal/Ca ratios are mean values for each site. Note Mg/Ca ratios are lowest in the Polar Mixed Layer, increase with depth through the Atlantic Layer [although the AL core is not well sampled] and Arctic Intermediate Water and decrease with depth below the AIW except for a few high values in the southern Eurasian Basin abyssal plain. Sr/Ca ratios decrease with water depth about 25 % in the Eurasian and Amerasian Basins. Bathymetry approximate.

Figure S4. MIS1 (red) and MIS3 (blue) Mg/Ca values for *K. glacialis* (left side) and *K. minima* (right side).

Figure S5. Downcore Mg/Ca and Sr/Ca values for *K. glacialis* (blue) and *K. minima* (red) from cores from Lomonosov Ridge (HLY0503-18tc, PS2185-4), Iceland Plateau (PS1243-1/2), Mendeleyev Ridge (P1-94AR-BC8, P1-94AR-BC19B), Gakkel Ridge (PS2163-1). Due to inverse relationship between Mg/Ca and Sr/Ca, X-axis scale is inverted for Sr/Ca curves. Despite different sedimentation rates and water depths, all cores show high values during pre-LGM late MIS3, decreasing post-LGM values, four cores had lower values during early MIS3 (HLY0503-18tc, PS2185-4, P1-94AR-BC19B, PS2163-1). Note similarity between Mg/Ca trends for *K. glacialis* and *K. minima* at sites where both species are present and negative correlation between Mg/Ca and Sr/Ca ratios ($r^2 = 0.50$ for *K. glacialis*, n=618; and $r^2 = 0.23$ for *K. minima*, n=209).

Figure S6. Vertical profiles of temperature and salinity from the Arctic Ocean at 82˚N taken in May 2002 by the AO-02 expedition (Rudels et al., 2005). This hydrographic station is representative for the water masses flowing southward and exiting the Arctic Ocean through the Fram Strait. The conceptual two-layer model is outlined in the left-hand panel. Its upper layer contains the near-freezing point waters in the Polar Mixed Layer and the cold halocline; the lower layer represents warmer Atlantic water.

Figure S7. Solutions of the two-layer model as a function of the freshwater input F. 2a shows the depth of the cold halocline, roughly corresponding to the depth of the 34.5 isohaline surface within the present-day Polar Surface Water. 2b shows the salinity difference between the Atlantic water and the halocline water. The black, blue, and red curves are obtained using an Atlantic water temperature of 1, 3, and 5˚C. For a sufficiently low layer density difference, the steady state solutions of the model become unstable. The unstable branch of the solutions is indicated with dashed lines.

References

Aagaard, K., L. K. Coachman, and E. C. Carmack. On the halocline of the Arctic Ocean. *Deep Sea Res*., **28A**, 529–545 (1981).

Backman, J. *et al.* Is the central Arctic Ocean a sediment starved basin? *Quat. Sci. Rev.* **23,** 1435-1454 (2004).

Chivas, A.R., De Deckker, P., & Shelley, J.M.G. Magnesium, strontium, and barium partitioning in nonmarine ostracod shells and their use in paleoenvironmental reconstruction- a preliminary study. In *Applications of Ostracoda* (ed. Maddocks, R.F.) 238-249, (Department of the Geosciences of the University of Houston, Houston, 1983).

Chivas, A.R., De Deckker, P., & Shelley, J.M.G. Magnesium and strontium in non-marine ostracod shells as indicators of palaeosalinity and palaeotemperature. *Hydrobiologia* **143,** 135-142 (1986).

Corrège, T. & De Deckker, P. Faunal and geochemical evidence for changes in intermediate water temperature and salinity in the western Coral Sea (Northeast

Australia) during the late Quaternary. *Palaeogeogr., Palaeoclimatol., Palaeoecol.* **131,** 183-205 (1997).

Cronin, T.M., Raymo, M.E., & Kyle, K.P. Pliocene (3.2-2.4 Ma) ostracode faunal cycles and deep ocean circulation. North Atlantic Ocean. *Geology* **24,** 695-698 (1996).

De Deckker, P., Chivas, A.R., & Shelley, J.M.G. Uptake of Mg and Sr in the euryhaline ostracod *Cyprideis* determined from in vitro experiments. *Palaeogeogr., Palaeoclimatol., Palaeoecol.* **148,** 105-116 (1999).

Dickson, B., B. Rudels, S. Dye, M. Karcher, J. Meincke, and I. Yashayaev. Current estimates of the freshwater flux through Arctic and subarctic seas. *Progress In Oceanography*, **73**, 210–230 (2007).

Dwyer, G.S. *et al.* North Atlantic deepwater temperature change during late Pliocene and late Quaternary climatic cycles. *Science* **270,** 1347-1351 (1995).

Dwyer, G. S., Cronin, T.M., & Baker, P.A. Trace elements in ostracodes. In *The Ostracoda: Applications in Quaternary Research* (eds Holmes, J.A., & Chivas, A.R.) 205-225 (Geophysical Monograph **131**, American Geophysical Union, Washington, DC, 2002).

Farmer, J., Cronin, T. M., & Dwyer, G.S. Ostracode Mg/Ca Paleothermometry in the North Atlantic and Arctic Oceans: Evaluation of the Carbonate Ion Effect. *Paleoceanogr*, **27**, PA2212, doi:10.1029/2012PA002305 (2012).

Held, I. M. and B. J. Soden. Robust response of the hydroligical cycle to global warming. *J. Clim*., **19**, 5686–5699 (2006).

Holmes, J. A. & Chivas, A. R. Ostracod carapace chemistry-overview. In *The Ostracoda: Applications in Quaternary Research* (eds Holmes, J.A., & Chivas, A.R.) 185-203 (Geophysical Monograph **131**, American Geophysical Union, Washington, DC, 2002).

Jakobsson, M. Hypsometry and volume of the Arctic Ocean and its constituent seas. *Geochem. Geophys. Geosyst.*, **3**, 1–18 (2002).

Jakobsson, M., J. Backman, B. Rudels, J. Nycander, M. Frank, L. Mayer, W. Jokat, F. Sangiorgi, M. O'Reagan, H. Brinkhuis, J. King, and K. Moran. The early Miocene onset of a ventilated circulation regime in the Arctic Ocean. *Nature*, **447**, 986–990 (2007).

Jakobsson, M., J. Nilsson, J. Backman, M. O'Regan, L. Löwemark, J. A. Dowdeswell, L. Mayer, L. Polyak, F. Colleoni, L. G. Anderson, G. Björk, D. Darby, B. Eriksson, D. Hanslik, B. Hell, C. Marcussen, E. Sellen, and Å. Wallin. An Arctic Ocean ice shelf during MIS 6 constrained by new geophysical and geological data. *Quat. Sci. Rev.*, **29**, 3505–3517 (2010).

Kato, M. and O. M. Phillips. On the penetration of a turbulent layer into a stratified fluid. *J. Fluid Mech.*, **37**, 643–655, 1969.

Nilsson, J. and G. Walin. Freshwater forcing as a booster of thermohaline circulation. Tellus, **53A**, 629–641 (2001).

Nilsson, J. and G. Walin. Salinity-dominated thermohaline circulation in sill basins: can two stable equilibria exist? *Tellus*, **62A**, 123–133 (2010).

Nørgaard-Pederson, N., Spielhagen, R. F., Erlenkeuser, H., Grootes, P. M., Heinemeier, J., Knies, J., 2003. Arctic Ocean during the Last Glacial Maximum: Atlantic and polar domains of surface water mass distribution and ice cover. *Paleoceanogr.*, **18**, 1063, doi:10.1029/2002PA000781.

Poirier, R. K., Cronin, T. M., Briggs, Jr., W. M., & Lockwood, R. Arctic paleoceanography for the last 50 kyr based on ostracode faunal assemblages. *Mar. Micropaleontol.* **88-89**, 65-76 (2012).

Polyak, L., Bischof, J., Ortiz, J. D., Darby, D.A., Channell, J. E. T., Xuan, C., Kaufman, D. S., Løvlie, R., Schneider, D. A., Eberl, D. D., Adler, R. E., Council, E. A. Late Quaternary stratigraphy and sedimentation patterns in the western Arctic Ocean. *Global and Planet. Change*, **68**, 5-17 (2009).

Polyak, L., Curry, W. B., Darby, D. A., Bischof, J., Cronin, T. M., 2004. Contrasting glacial/interglacial regimes in the western Arctic Ocean as exemplified by a sedimentary record from the Mendeleev Ridge. Palaeogeography, Palaeoclimatology, Palaeoecology, **203**, 1-2, 73-93 (2004).

Rudels, B. The thermohaline circulation of the Artic Ocean and the Greenland Sea. *Phil. Trans. R. Soc. Lond.*, **352**, 287–299 (1995).

Rudels, B., G. Björk, J. Nilsson, P. Winsor, I. Lake, and C. Nohr. The interaction between waters from the Arctic Ocean and the Nordic Seas north of the Fram

279 Strait and along the East Greenland Current: results from the AO-02 Oden
280 expedition. *J. Mar. Systems*, **55**, 1–30 (2005).
281 Stigebrandt, A. A model for the thickness of and salinity of the upper layer in the Arctic
282 Ocean and the relationship between the ice thickness and some external
283 parameters. *J. Phys. Oceanogr.*, **11**, 1407–1422 (1981).
284 Stuiver, M., Reimer, P., 2010. CALIB 6.0.1 Reservoir Corrections program. Available
285 online at: http://calib.qub.ac.uk/calib/
286 Turpen, J. B., & Angell, R. W. Aspects of molting and calcification in the ostracod
287 *Heterocypris*. *Biol. Bull.* **140,** 331-338 (1971).
288

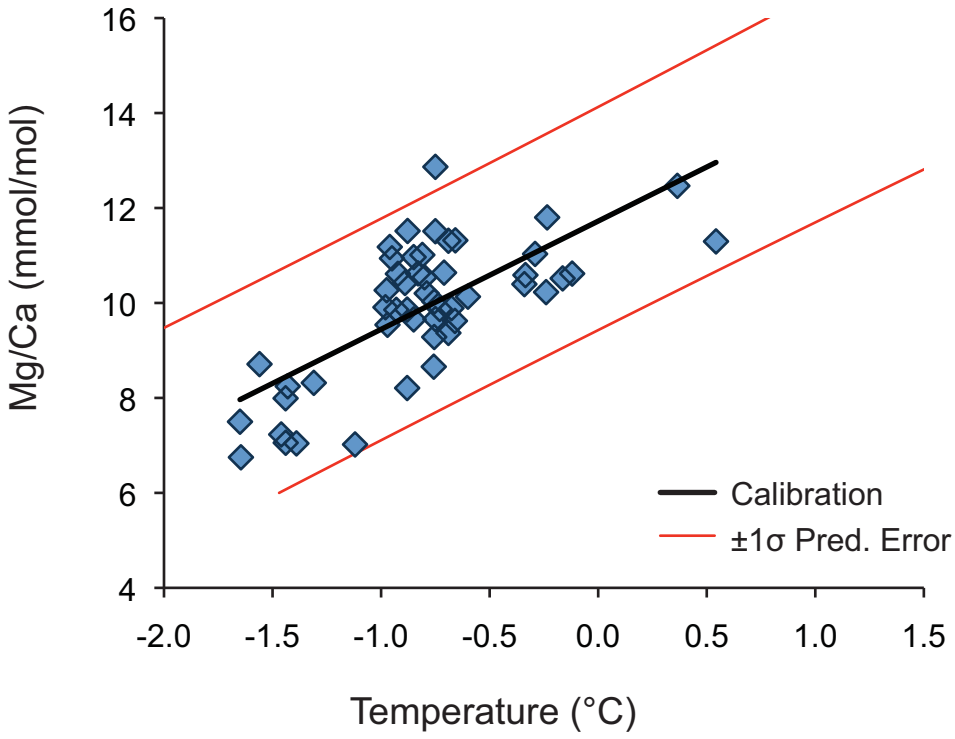

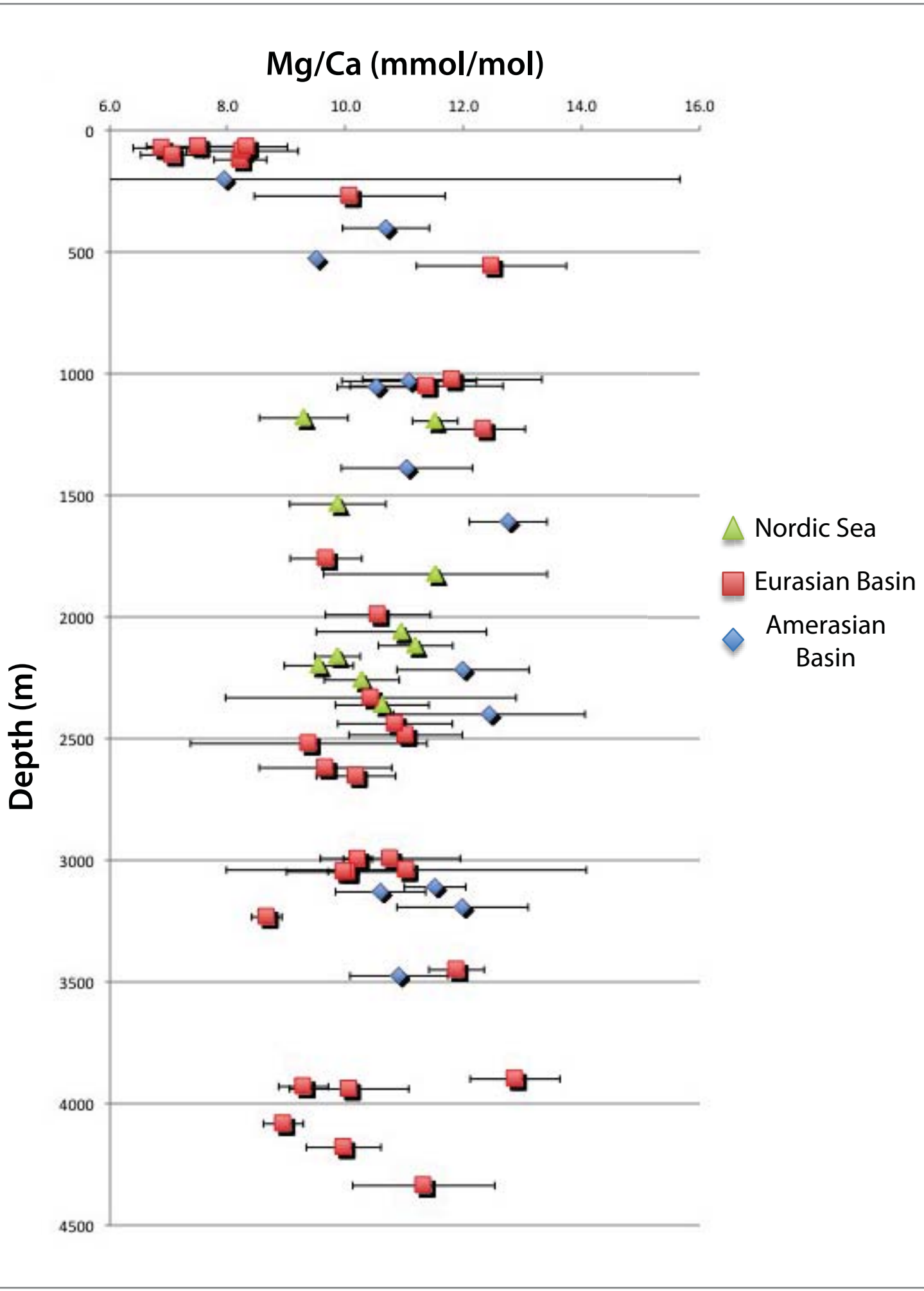

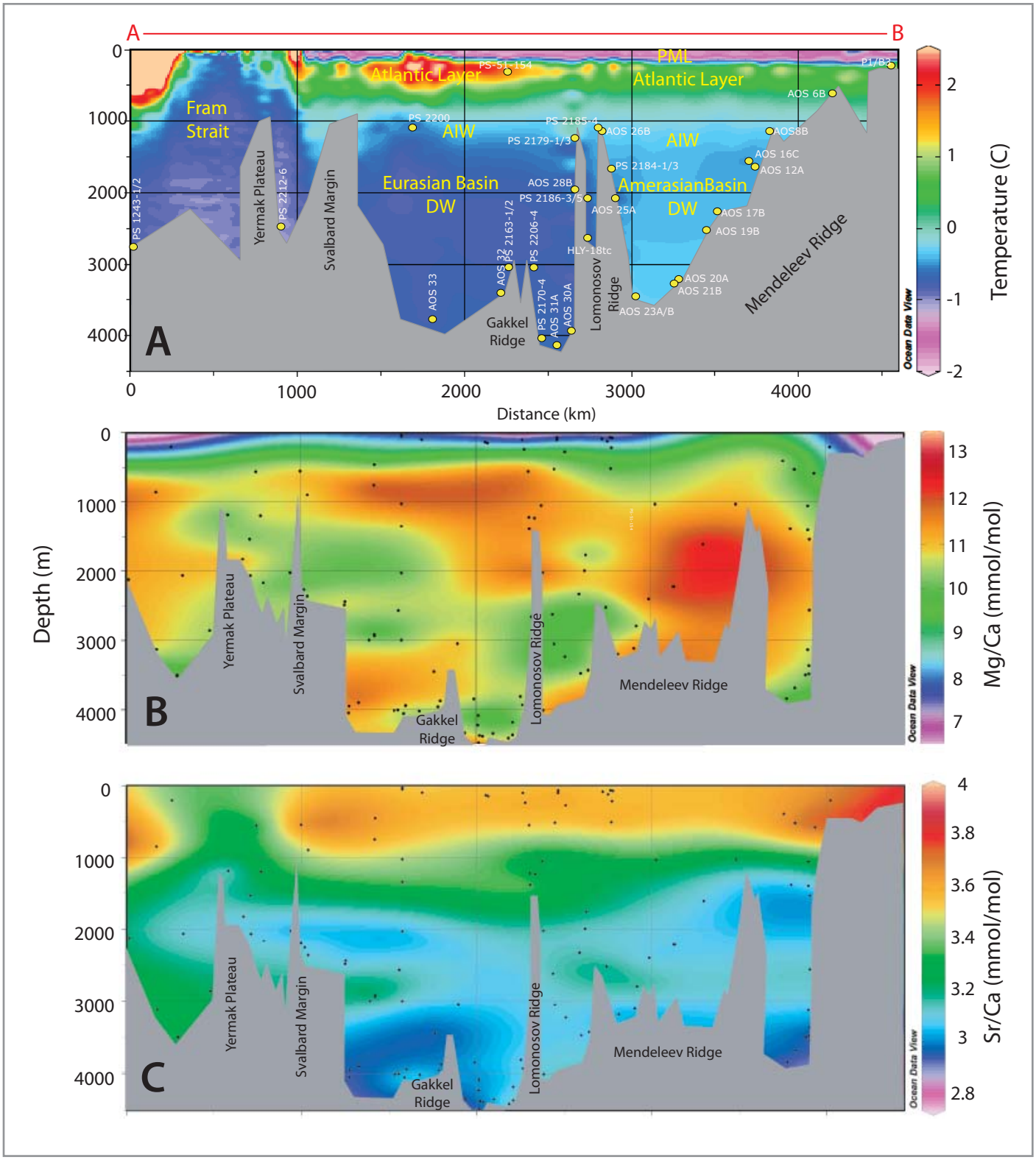

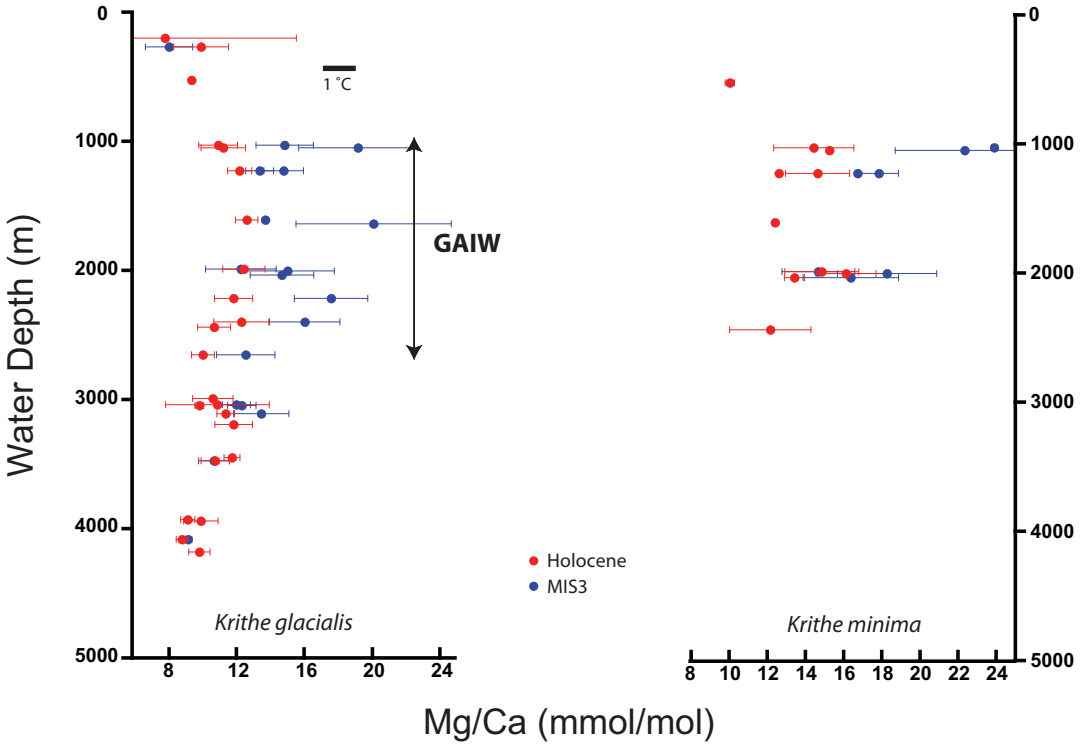

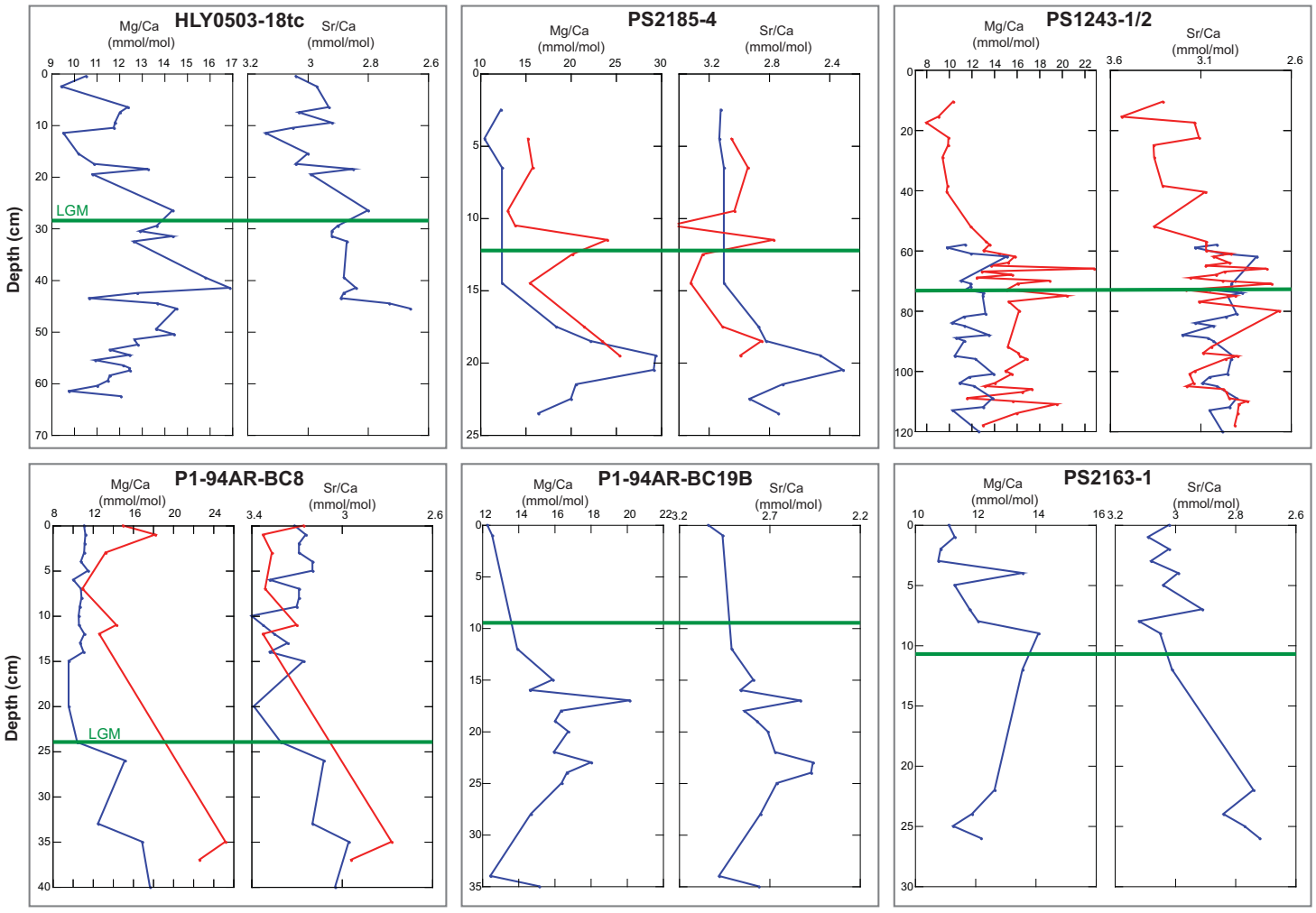

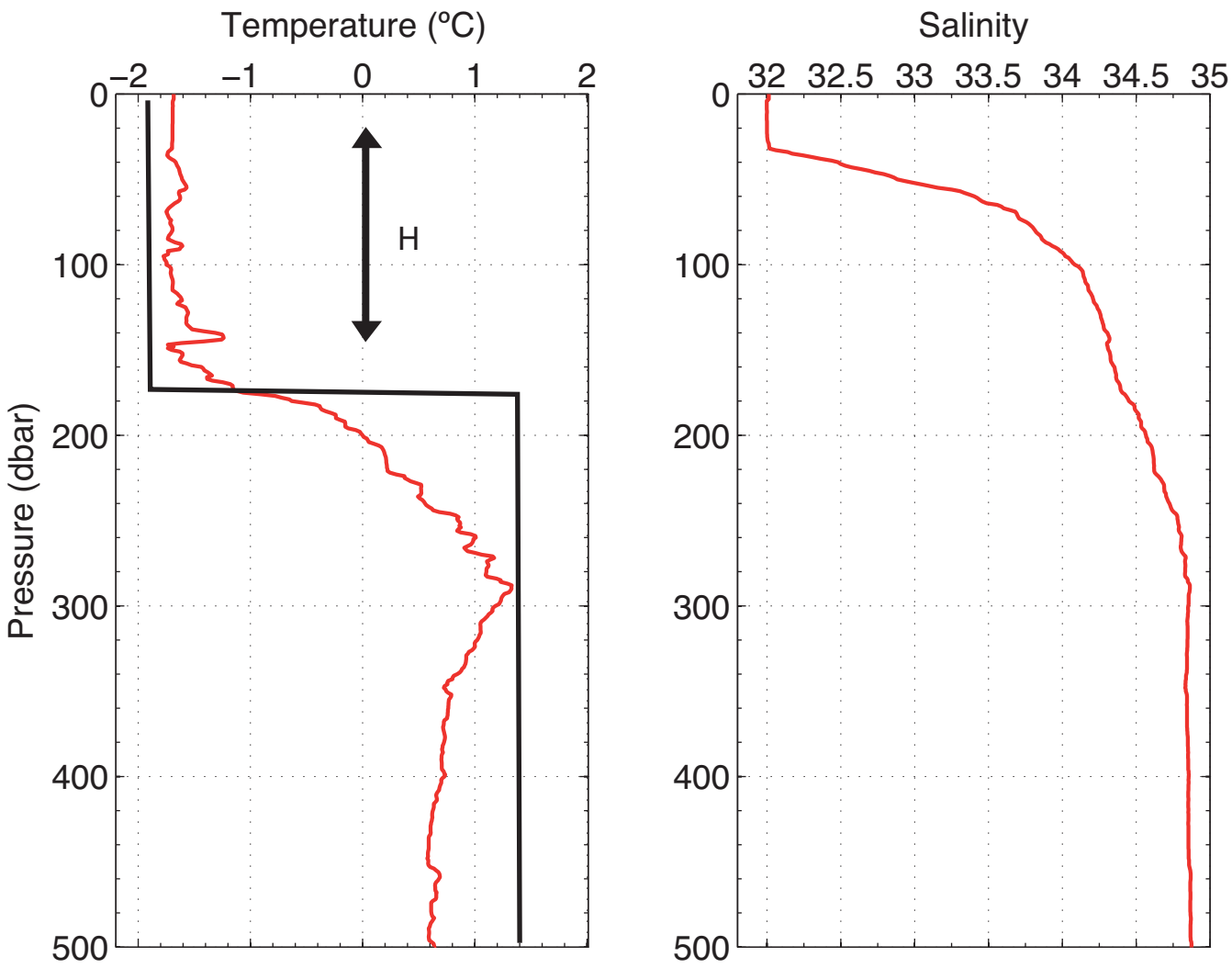

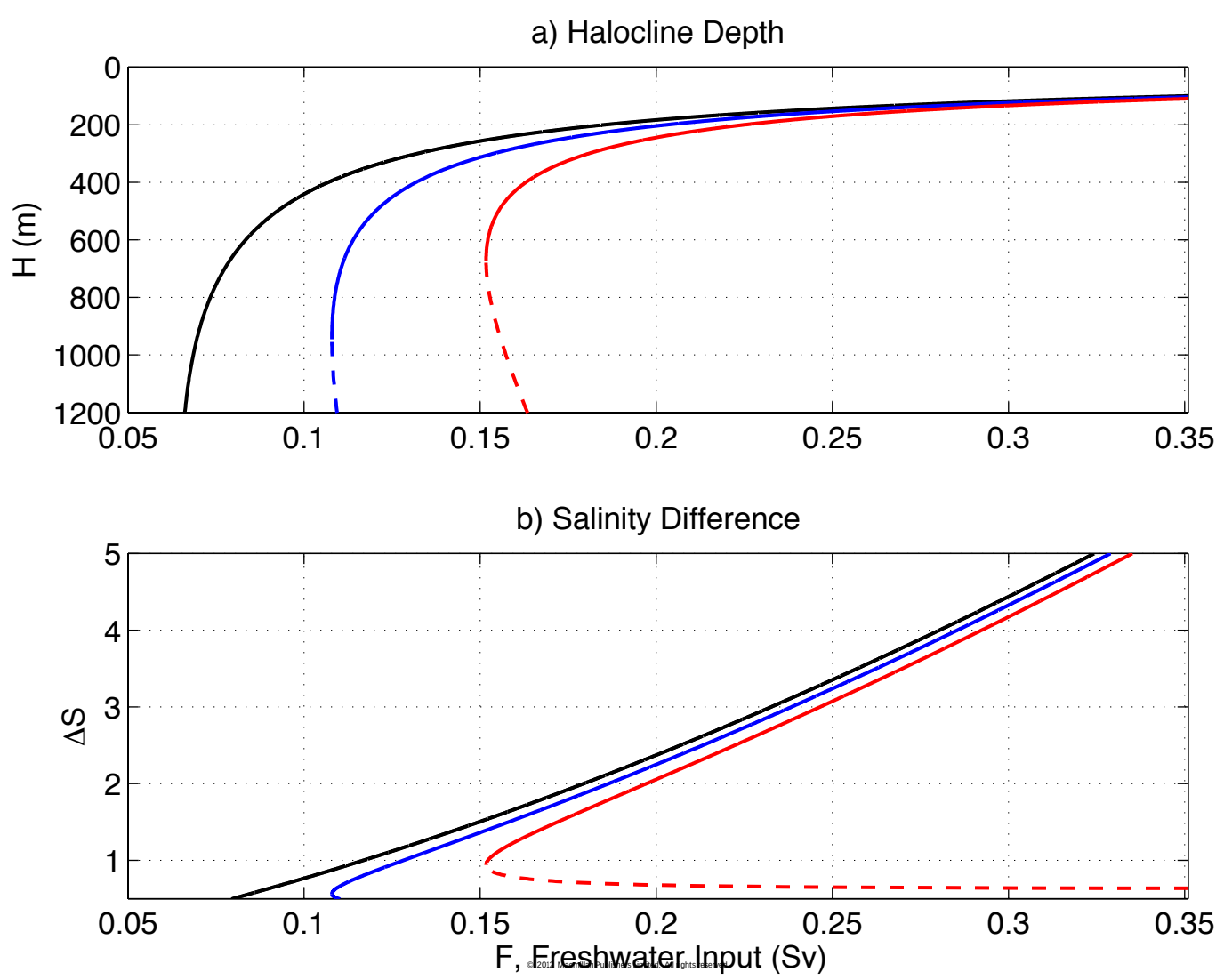
a) Halocline Depth
H (m)
0
200
400
600
800
1000
1200
0.05
0.1
0.15
0.2
0.25
0.3
0.35
b) Salinity Difference
ΔS
5
4
3
2
1
0.05
0.1
0.15
0.2
0.25
0.3
0.35
F, Freshwater Input (Sv)